High-efficiency Removal of Diclofenac via Advanced Technologies: A Comparative Study of Photocatalysis, Adsorption, and Nanofiltration

Nabil Jallouli, FeryelleAouay, Mohamed Romdhani & Raja Ben Amar*

Research Unit "Advanced Technologies for Environment and Smart Cities", Faculty of Sciences, University of Sfax, 3000 Sfax, Tunisia

ABSTRACT

Pharmaceuticals are frequently detected in the environment due to their partially removal by the conventional wastewater treatment processes. In order to limit their accumulation in the environment, effective tertiary treatments must be employed. In the present study, the removal of Diclofenac (DCF), a nonsteroidal anti-inflammatory drug (NSAID) using three advanced water treatment technologies, i.e., photocatalysis, adsorption by activated carbon (AC) and nanofiltration (NF) was investigated. Titanium dioxide (TiO_2) was used as a photocatalyst for the degradation of DCF and a removal of 100% was observed in the optimal conditions (pH= 5, Dose of TiO_2=1 g. L^{-1} and [DCF]= 20 mg.L^{-1}). Spent coffee grounds (SCG) as the AC exhibited a capacity of adsorption of 100 mg.g^{-1}, contributing to 100% removal of DCF. On the other hand, the removal of DCF by NF membrane showed a high retention of 97% at 4 bars and reached 100% at 6 and 8 bars. A comparison between these three methods has shown that photocatalysis offers fast, complete pollutant degradation without secondary pollution and adsorption is cost-effective while NF is effective but challenged by fouling and waste issues. This study highlights effective and practical solutions for removing DCF from water, offering promising options to improve wastewater treatment and reduce pharmaceutical pollution.

Keywords: Diclofenac, Photocatatalysis, TiO_2, adsorption, spent coffee grounds, Nanofiltation

1.0 INTRODUCTION

Pharmaceuticals are considered as emerging contaminants due to their widespread use in human and veterinary medicine and their occurrence in the environment is reported by many researchers [1, 2]. Diclofenac (DCF) is considered as a persistent emerging contaminant and was detected in surface water, ground water and sewage treatment plants [3-5]. The accumulation of this drug in the environment poses a risk to the aquatic organisms and can cause endocrine-disruption [6-9]. Conventional wastewater treatment processes are not designed to remove pharmaceutical residues such as DCF

and their removal is incomplete up to 40% for DCF [10, 11].

To remediate the limitations of conventional treatment methods, adsorption, membrane technology, and advanced oxidation processes (AOPs) have emerged as effective techniques for removing these recalcitrant contaminants in recent years [12]. Among the AOPs, photocatalysis process employs a photocatalyst irradiated with a UV or visible light to produce radicals, very efficient to degrade organic compounds such as DCF [13, 14]. TiO_2 is a widely used semiconductor because of its high stability, nontoxic nature and its low cost [15].

Membrane process is considered as a promising technology for the water treatment and separation processes [16]. This process has many advantages such as low power consumption, efficiency and high separation [17]. According to their pore size, membranes are classified as microfiltration (MF), ultrafiltration (UF), nanofiltration (NF) and reverse osmosis (RO). NF is capable of rejecting molecules in order of one nanometer in size such as micropollutants [18]. Besides NF is advantageous because of its lower operating pressure compared to RO and its low investment costs [19]. These features allow NF to be utilized in the removal of pharmaceuticals from water and wastewater [20]. Studies have reported the removal of various emerging contaminants by NF such as paracetamol, naproxen or anticancer drugs such as paclitaxel and etoposide [21, 22].

AC is an emergent adsorbent that has many advantages such as low cost, ease of application and the possibility of regeneration [23, 24].Coffee is one of the world's most consumed beverages, with more than five million tons produced annually according to a 2022 report released by the International Coffee Organization, London, UK. Spent coffee grounds (SCG) are typically discarded through composting, incineration, or landfilling, practices that may release residues of tannins, caffeine, and polyphenols with negative environmental impacts. SCG is a major waste product, with millions of tons produced from coffee consumption each year. Due to their high organic content, they are a valuable resource that can be utilized in a variety of applications such as the AC [25, 26]. Previous studies reported the removal of emerging contaminants including DCF by AC [27, 28]

The removal of an emerging contaminant, carbamazepine by the three methods using the reduced graphene oxide as adsorbent, TiO_2-reduced graphene oxide (rGO) as photocatalyst and UF was compared in a previous work [29]. To the best of our knowledge, a study combining these three methods of treatment including TiO_2 photocatalysis, SCG and NF is missing in the literature.
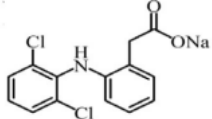
In this study, the DCF removal was carried out by applying three different processes, i.e., photocatalysis, adsorption and NF. The comparison between these processes was conducted. The innovative aspect of this work lies in the comparison studies using advanced techniques for wastewater treatment and coffee waste as adsorbent which contributes also to waste management. This study contributes to environmental preservation efforts while promoting the reuse of organic waste, presenting practical approaches to enhance the efficiency of wastewater treatment.

2.0 MATERIALS AND METHODS

2.1 Chemicals:

DCF was supplied from the pharmaceutical manufacturer Dar Essaydali. Titania P25 Degussa (TiO_2; ca. 80% anatase and 20% rutile) was purchased from Sigma-Aldrich.The Phosphoric acid (H_3PO_4, 80%) and was used as the activating agent to prepare the AC. The pH was adjusted with H_2SO_4 (0.1 M) and NaOH (0.1 M). Ultrapure (UP) water was supplied by a Milli-Q water system.

Table 1 Physical and chemical properties of DCF

Molecular structure	Molecular formula	Molecular weight (g/mol)	Solubility (g/L)	pKa	Surface area (nm^2)	Molecular size (nm)
	$C_{14}H_{10}Cl_2NNaO_2$	318.1	4.82	4.15	0.52	0.98

2.2 Analytical Methods

The evolution of DCF concentration was determined by a UV–vis double beam PC scanning spectrophotometer at a wavelength of 275 nm.

2.3 Synthesis of AC

2.3.1 Preparation Method

The AC was prepared from SCG according to the study of Aouay *et al.* [25]. Typically, 20 g of SCG were washed and dried in the oven at 60°C. The obtained SCG were immersed in a solution of H_3PO_4 (80%) and stirred for 3 h at 80°C. A slow pyrolysis was then carried out at 600°C in a muffle furnace for 2 h. The obtained ACs were finally washed with UP water to a neutral pH and dried at 105°C in an oven for 24 h. After activation, the ACs were crushed and sieved. The fraction used for testing was < 100 μm.

2.3.2 Characterization of ACs

The surface morphology of the ACs before and after DCF adsorption was examined using scanning electron microscopy (SEM, Hitachi S4800, Tokyo, Japan) to observe potential changes in surface texture and porosity. Additionally, Fourier transform infrared (FTIR) spectroscopy (Spectrum 100, Perkin Elmer, Waltham,

MA, USA) was employed to identify the functional groups present on the AC surface and detect any modifications following DCF adsorption.

2.3 Adsorption Study

2.3.1 Adsorption Experiments

The adsorption tests were carried out by adding a certain amount of AC to 100 mL of solution of DCF from a stock solution (0.1 g.L^{-1}) under magnetic stirring. The different concentrations needed for the adsorption experiments were prepared by dilution with UP water.

2.3.2 Adsorption Kinetics and Isotherm Experiments

Kinetic and isotherm experiments were conducted to evaluate the adsorption performance of AC for DCF removal. The adsorption kinetics were studied by adding a fixed amount of AC (0.2 g. L^{-1}) to a DCF solution of a concentration of 20 mg. L^{-1}. The mixture was stirred at room temperature and samples were withdrawn at predetermined time intervals to determine DCF concentration using UV-vis spectrophotometry. The kinetic data were analyzed using the pseudo-first-order (PFO) and pseudo-second-order (PSO) models, given by the following equations:

$$\text{Ln } (q_e - q_t) = \text{Ln } (q_e) - k_1 t \qquad (1)$$

$$\frac{t}{q_t} = \frac{1}{k_2 \cdot q_e^2} + \frac{t}{q^e} \qquad (2)$$

where q_t and q_e are the adsorption capacities at time 't' and at equilibrium, respectively, k_1 is the pseudo-first-order rate constant (min^{-1}), and k_2 is the pseudo-second-order rate constant ($g\ mg^{-1}\ min^{-1}$).

Adsorption isotherm experiments were performed by equilibrating DCF solutions with AC at different initial concentrations ranging from 10 to 100 mg. L^{-1} while keeping the AC dosage (0.2 g. L^{-1}) and contact time constant. Langmuir and Freundlich isotherm models are the most widely used isotherms due to their simplicity and clarity (Eq. (3) for langmuir model and Eq (4) for Freundlich model).

$$\frac{Ce}{qe} = \frac{1}{Kl.qmax} + \frac{Ce}{qmax} \qquad (3)$$

$$\text{Log } q_e = \log k_f + \frac{1}{n}.\log C_e \qquad (4)$$

where C_e ($mg.L^{-1}$) the concentration at of DCF at equilibrium, q_e ($mg.g^{-1}$) is the adsorption capacity of AC at equilibrium, q_{max} is the maximum adsorption capacity of the AC and equilibrium. K_F is the Freundlich constant and K_L is the Langmuir constant ($mg.\ L^{-1}$).

2.4 Photocatalytic Degradation of DCF

The photocatalytic experiments of DCF were conducted in in a lab-scale photoreactorwith a capacity of 0.3L. The reactor was equipped with an 18 W UV A lamp (Philips). In a typical run, the reactor, maintained under magnetic stirring and aeration, was filled with a 200 ml of DCF solution (10, 20, 30 or 40 mg. L^{-1}) and a given amount of TiO_2 (0.5,1 ,1.5, 2 and 3 g. L^{-1}). The suspension was kept 30 min in the dark before switching on the lamps under magnetic stirring for the adsorption/desorption phase. At predetermined time intervals, 3-mL aliquots were collected and filtered with syringe filters (0.45-µm pore size).

2.5 Nanofiltration experiments

A test bench provided by PTE (Water Purification and Treatment) was employed. In this process, NF 270 membrane was used with a feed tank of 30 L of capacity. A circulation pump (VEMAT model VMB 71 B, Italy) maintained the transmembrane pressure (TMP)at the operating pressures : 4,6 and 8 bars and at an ambient temperature of 25°C controlled by a cooling system to maintain the thermal stability[30] for a feed solution containing of 20 mg. L^{-1} DCF.

Table 2 Membrane's characteristics

Area (m^2)	Cut-off (Da)	Material	Manufacturer	Pure water permeability ($L/m^2.h.bar$)
1.2	200 (NF270)	Polyamide	Dow Filmtec, Santa Ana, CA, United States	7.6 ± 0.2

3.0 RESULTS AND DISCUSSION

3.1 Photocatalytic degradation of DCF

3.1.1 *Effect of TiO₂ Loading*

The photocatalytic degradation of DCF was assessed using various amounts of TiO_2 catalysts at natural solution pH (5.3). Figure 1 shows apparent pseudo-first-order rate constants (k_{app}) of DCF degradation at different photocatalyst load (0.5, 1, 1.5, 2 and 3 g. L^{-1}). DCF degradation significantly increased with the catalyst load until 1 g. L^{-1} (k_{app}= 0.0048 min^{-1}). Afterwards, a decrease in DCF degradation was observed with the increase in TiO_2 loading from 1 to 3 g.L^{-1} reaching k_{app}= 0.0025 min^{-1}. It is well known that the degradation rate in photocatalysis does not increase after a certain catalyst load may be due to light scattering [31].
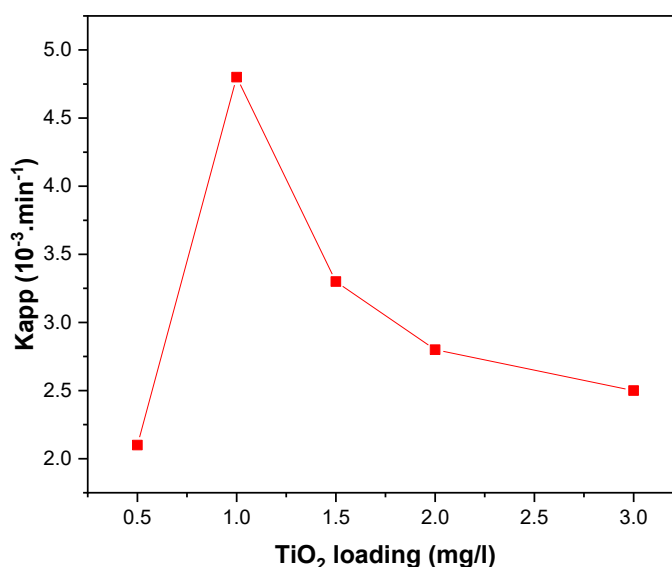

Figure 1 Effect of the catalyst loading on the DCF photocatalytic degradation

3.1.2 *Effect of DCF Initial Concentration*

The photocatalytic degradation efficiency is also largely influenced by the amount of initial pollutant concentration. To study the impact of the initial DCF concentration, solutions of diclofenac were utilized in photocatalytic degradation experiments, with various concentrations (ranging from 10 to 40 mg. L^{-1}) and with a constant amount of catalyst dosage (1g.L^{-1}) at natural pH (Figure 2). The degradation rate of DCF decreases from 10 to 20 mg. L^{-1}. This decrease becomes drastically important when the initial concentration increased to 40 mg. L^{-1} (62% removal after 180 min) due to the reduction in the available surface area of the catalyst surface [32].As a result, the formation of hydroxyl radicals may be reduced to a level that impacts the photocatalytic activity of the catalysts [33].
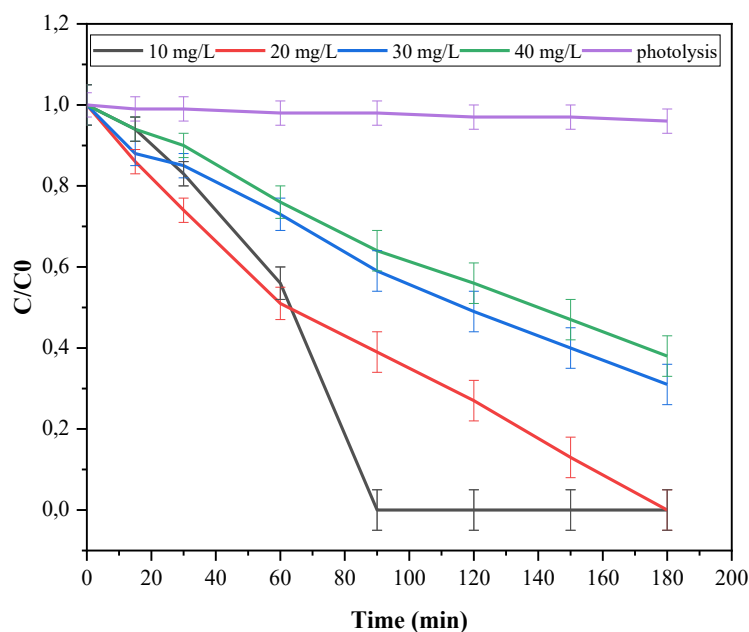
Figure 2. Effect of initial DCF concentration onits photocatalytic degradation

3.1.3   Effect of Initial pH

The photocatalytic degradation of DCF was investigated by varying the initial pH solution of DCF from 3 to 11 and the results are shown by Figure 3. As observed, the highest degradation rate was achieved at the natural pH (5.3). This result is attributed to the point of zero charge pH_{PZC} of TiO_2 (6.6) and the pKa of DCF (4.2). At pH 3.0, the interaction between the DCF molecules and the photocatalyst surface is reduced because DCF molecules are undissociated below their pK_a of 4.9, while the TiO_2 surface is positively charged, which decreases the electrostatic attraction. At natural pH=5, DCF molecules are negatively charged, whereas the TiO_2 surface is positively charged, as indicated by its pH_{PZC} (6.6) which enhances the electrostatic attraction between the positively charged TiO_2 surface and the negatively charged DCF molecules. In this case, the photocatalytic degradation increased. On the other hand, at pH=11, lower photocatalytic degradation was observed. It can be explained by the electrostatic repulsion of DCF molecules and the TiO_2 surface both negatively charged when the pH is above 6.6. Some authors reported similar findings [33].
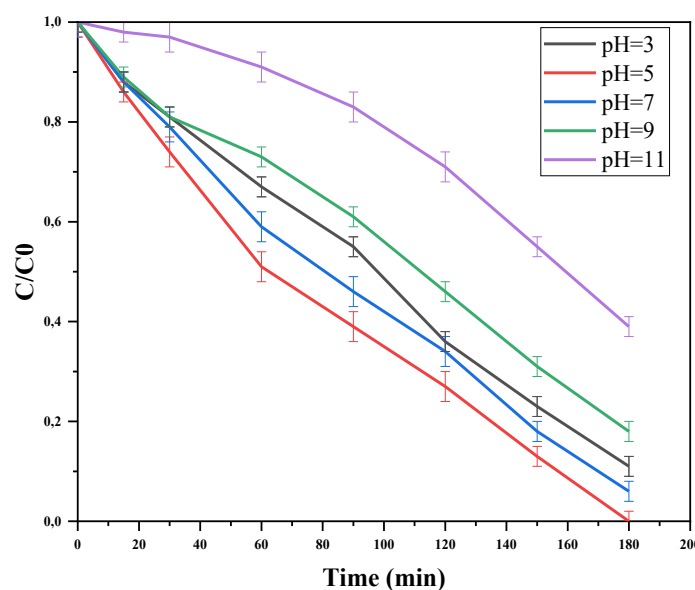
Figure 3 Effect of solution pH on the DCF photocatalytic degradation as a function of time

3.2 Adsorption of DCF on AC

3.2.1 Characterization Studies

Various techniques were employed to study the characteristics of the AC and mechanisms of DFC adsorption. In this study, scanning electron microscopy (SEM) was used to observe the surface morphology of AC before and after DCF adsorption. The micrograph before adsorption (Figure 4(a)) reveals a highly porous and rough surface, with numerous cavities and well-developed channels. This confirms the effectiveness of the activation process in generating a large specific surface area favorable for adsorption.

After adsorption (Figure 4(b)), the surface of the AC appears smoother and many of the pores seem partially or totally blocked. This morphological change suggests that DCF molecules have been adsorbed onto the surface and into the pores of the AC, leading to the partial clogging of the porous structure. The reduction in visible porosity and surface roughness provides visual confirmation of successful DCF adsorption onto the AC surface. These observations are

consistent with the results obtained from the adsorption experiments, confirming the affinity between DCF and the functionalized surface of the AC.

These observations are consistent with the results obtained from the adsorption experiments, confirming the affinity between DCF and the functionalized surface of the activated carbon.

The FTIR spectrum of pristine AC aligns with previous findings reported by Aouay *et al.* [25], confirming the presence of characteristic oxygenated functional groups. As shown in Figure 5, a broad absorption band in the 3300–3500 cm^{-1} region corresponds to O–H stretching vibrations, indicating the presence of hydroxyl groups and adsorbed water molecules. The peak observed at 1600 cm^{-1} is attributed to C=O stretching from carboxyl or quinone groups, which are known to enhance adsorption capacity. Additionally, bands in the 1100–1250 cm^{-1} range correspond to C–O stretching vibrations, further supporting the presence of oxygen-containing functionalities that contribute to the surface reactivity of AC [25]. After

DCF adsorption, significant modifications in the spectrum were observed. Indeed, the intensity of the O–H stretching band decreased, suggesting hydrogen bonding interactions between DCF and the AC surface; the C=O stretching band at 1600 cm⁻¹ exhibited a slight shift, indicating π–π interactions between the aromatic rings of DCF and the graphitic structure of carbon-graphene AC [34]. The emergence of new absorption bands in the 1400–1500 cm⁻¹ range suggests electrostatic interactions between the negatively charged DCF molecules and the positively charged functional groups on AC [35]. These spectral changes confirm the involvement of multiple adsorption mechanisms, including hydrogen bonding, electrostatic attraction, and π–π interactions. The results are consistent with previous studies on DCF adsorption onto biochar-based adsorbents [36].
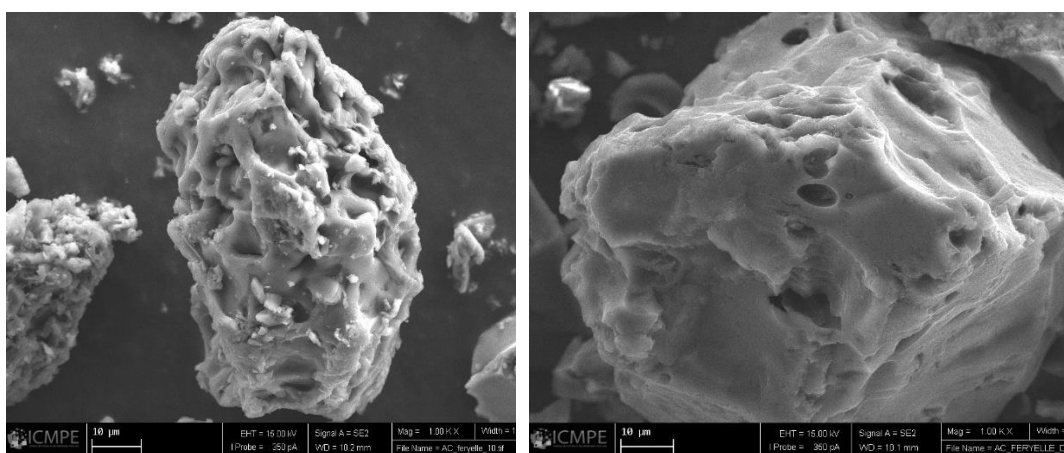

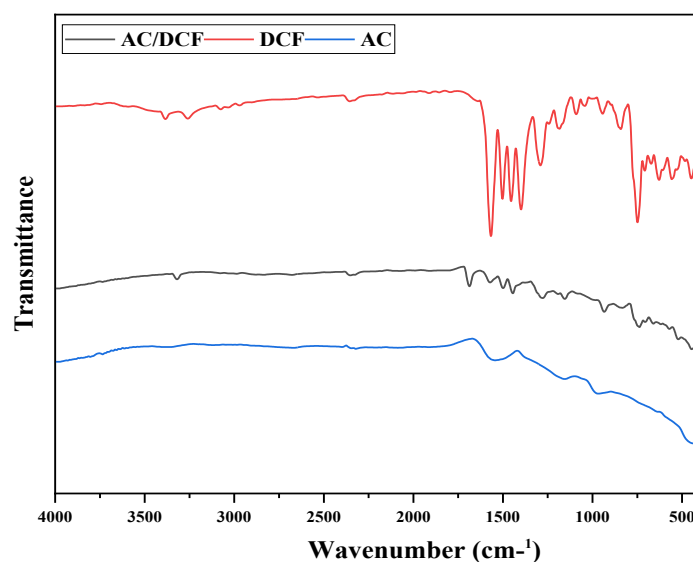**Figure 4** SEM micrographs of activated carbon before (left) and after (right) DCF adsorption

Figure 5 Comparison of the FTIR spectrum of DCF, AC and AC after DCF adsorption (AC/DCF)

3.2.2   Effect of AC loading

The effect of AC dosage on DCF removal efficiency was investigated by varying the adsorbent concentration from 0.1 to 0.4 g. L^{-1}, at a constant DCF concentration of 20 mg. L^{-1} and temperature of 25 °C (Figure 6). As anticipated, the removal efficiency of DCF increased with the AC dosage. This enhancement can be attributed to the greater surface area and higher number of available adsorption sites provided by the increased amount of AC, facilitating more interactions between DCF molecules and the adsorbent[35]. The improved performance with higher AC dosage is mainly due to the enhanced accessibility of active binding sites for DCF uptake from the aqueous phase.
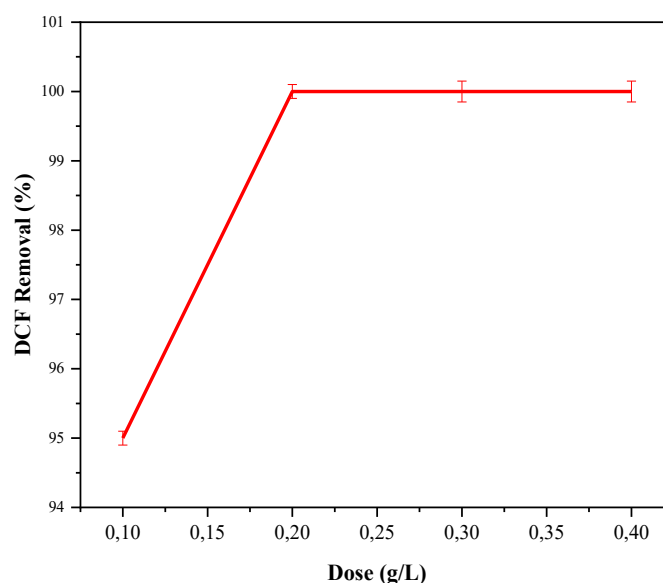

Figure 6 Effect of adsorbent dosage on DCF adsorption under conditions: [DCF]= 20 mg. L^{-1}, temperature = 25 °C, contact time = 60 min, and pH = natural (5)

3.2.3   Effect of DCF Initial concentration

The influence of initial DCF concentration on adsorption performance onto AC was evaluated by maintaining a constant adsorbent dose of 0.2 g. L^{-1}, as shown in Figure 7. The results indicate that DCF removal efficiency decreases progressively as the initial DCF concentration increases. This trend is due to the number of available active sites on AC which become rapidly saturated at high DCF concentrations leaving excess DCF molecules unadsorbed in the solution. Consequently, the removal efficiency declined from 100% to 89%. The high removal rate observed at lower DCF concentrations is attributed to the greater availability of active adsorption sites, which promotes easier interaction and binding of DCF molecules to the adsorbent surface.
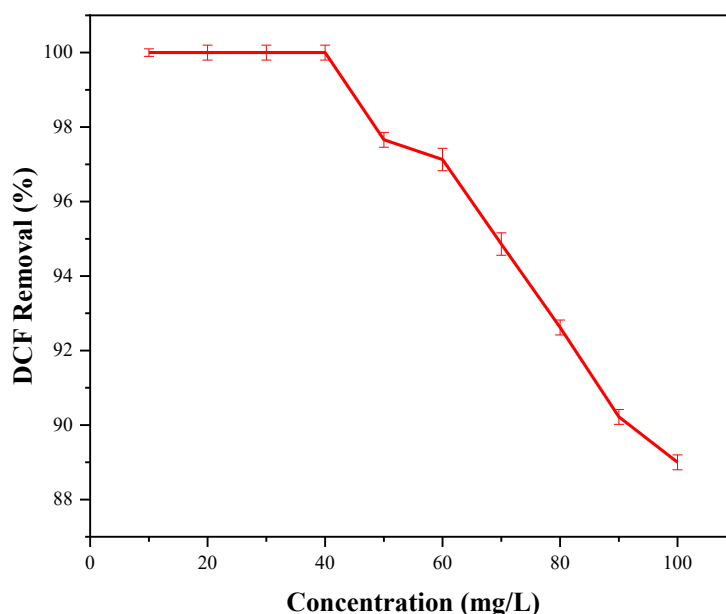
Figure 7 Effect of initial DCF concentration under the following conditions: AC dosage = 0.2g. L^{-1}, contact time = 60 min, and pH =natural (5)

3.2.4   Effect of Initial pH

The impact of pH on DCF adsorption onto AC was assessed over a pH range of 1 to 10, while maintaining a constant initial DCF concentration of 20 mg. L^{-1} and an adsorbent dose of 0.2 g. L^{-1}, the pH of each solution was adjusted at 25 °C. As shown in Figure 8, the removal efficiency of DCF decreases progressively with increasing pH. The point of zero charge (pH$_{pzc}$) of the AC was previously determined to be 2.4 [25]. At pH values below this threshold, the surface of the AC carries a positive charge, which favors electrostatic attraction with DCF species. Since the pK$_a$ of DCF is approximately 4.2, the molecule predominantly exists in a neutral form below this pH and becomes negatively charged as the pH increases above 4.2 due to deprotonation. This explains the higher affinity of AC for DCF under acidic conditions. As the pH exceeds the pH$_{pzc}$, both the adsorbent surface and DCF molecules acquire negative charges, resulting in increased electrostatic repulsion and thus a significant decline in adsorption capacity. When the pH increases from 3 to 10, the removal efficiency deceases significantly from 100% to 29%, confirming that acidic conditions are more favorable for DCF adsorption onto AC.
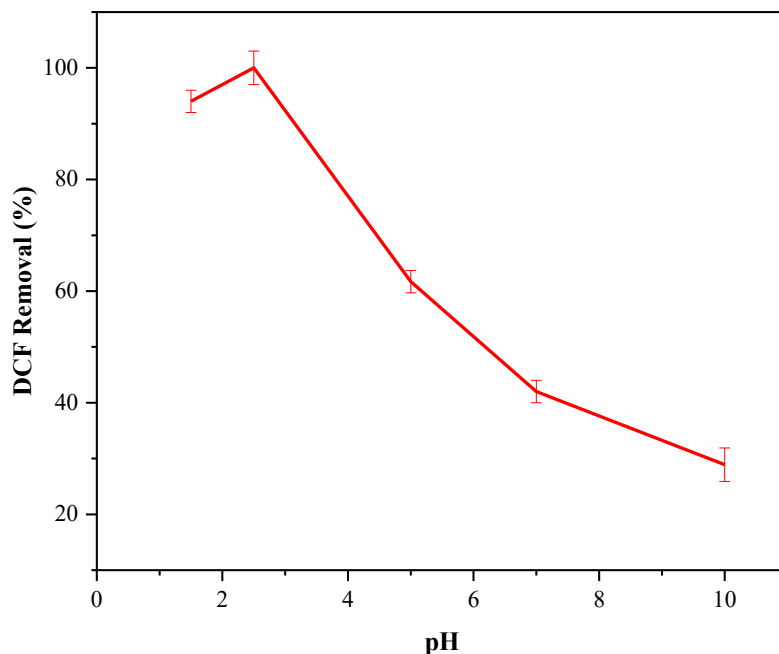
Figure 8 Effect of pH solution on DCF adsorption under conditions: AC dosage = 0.2g. L^{-1}, [DCF]= 20 mg.L^{-1}, temperature = 25 °C, contact time = 60 min

3.2.5   *Adsorption Kinetics*

The study of adsorption kinetics and equilibrium is essential for understanding and optimizing the adsorption process. The retention rate

of DCF by AC was examined to determine the most suitable kinetic model. Figure 9 presents the experimental results fitted to two theoretical approaches: the PFO model and the PSO model.
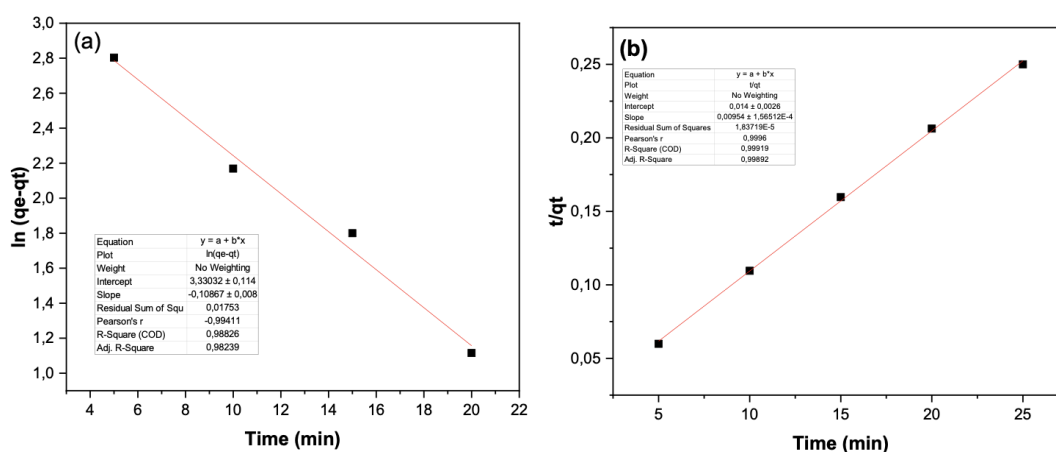

Figure 9 Kinetic plots and fitted kinetic model curve for DCF adsorption on AC: (a) pseudo-first-order kinetic and (b) pseudo-second-order models

The kinetic model parameters are summarized in Table 3. The results indicate that the experimental data fit

the PSO model better, with a determination coefficient R² close to unity. Additionally, the experimentally

determined adsorbed quantity ($q_e = 100$ mg.g^{-1}) is very close to the calculated value ($q_e = 104.82$ mg.g^{-1}). These results confirm that the PSO model accurately describes the adsorption kinetics of DCF on AC, in agreement with previous studies on DCF adsorption[37].

A deeper analysis shows that the PSO model's fit is logical since

chemical adsorption is often involved in DCF interaction with the activated carbon surface[38]. The PFO model, which assumes physical adsorption limited by diffusion, does not match the experimental data, confirming that chemical interactions primarily govern DCF adsorption on AC[39].

Table 3 Kinetic parameters for DCF adsorption

Models	Pseudo – first order			Pseudo – second order		
Coefficient	K_f (min^{-1})	q_e (mg.g^{-1})	R^2	K_s (mg.(g.min)$^{-1}$)	q_e (mg.g^{-1})	R^2
Q_{exp} mg.g^{-1} =100	-0.00434	27.95	0.98	0.0065	104.82	0.998

3.2.6 Adsorption isotherms of DCF on AC

The determination of adsorption isotherms is crucial for understanding the interactions between DCF molecules and the AC. The experimental results are shown in Figure 10, with the fitted theoretical curves. The optimized parameter values are summarized in Table 4. The analysis reveals that the Freundlich model provides a better fit to the experimental data ($R^2 = 0.977$) compared to the Langmuir model ($R^2 = 0.9430$). These

results suggest from the experimental data to conclude that the adsorbent surface is heterogenous, promoting multilayer adsorption [40]

The Freundlich model interpretation, although less suitable, indicates a degree of surface heterogeneity of the activated carbon, which can be consistent with some observed experimental variations. The 1/n factor in the Freundlich model being less than 1 (0.296) confirms a favorable adsorption, which aligns with the good performance of the studied AC [41].
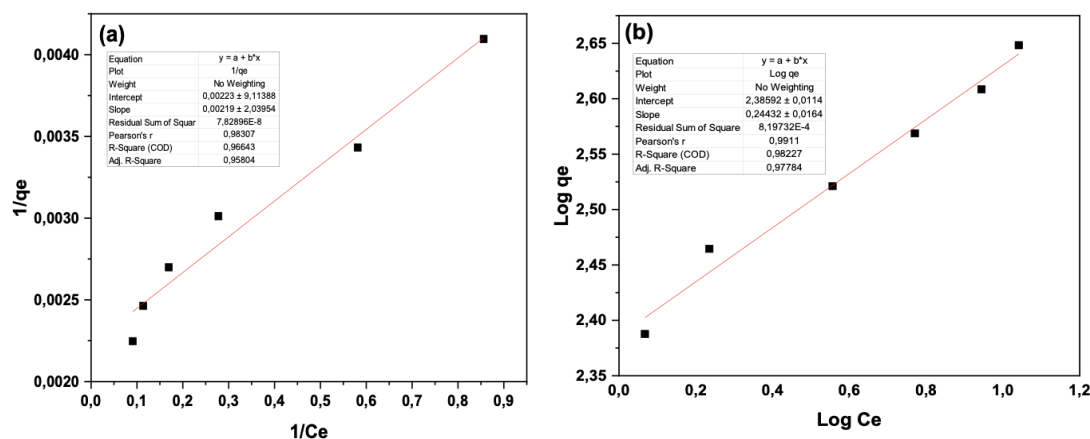

Figure10 The adsorption isotherms of DCF along with matched lines obtained with (a) Langmuir model and (b) Freundlich model

Table 4 Isotherm modeling parameters

Models	Langmuir				Freundlich		
Parameters	K_L(L.mol^{-1})	q_{max}(mg.g^{-1})	R²	R_L	K_F (L.g^{-1})(L.mg^{-1})$^{1/n}$	1/n	R²
Q_{max} : 445 mg.g^{-1}	1.018	448.43	0.958	0.00972	243.176	0.24432	0.977

The adsorption performance of the AC obtained in this work was compared with that of other adsorbents previously reported for DCF removal. The comparison includes biochars, chemically activated carbons, graphene-based materials, metal organic frameworks (MOFs) and zeolites, which differ strongly in surface area, functionalization, and synthesis cost.

3.2.7 Comparative study

Table 5 shows that the adsorption capacities reported for DCF removal vary widely, ranging from less than 38.5 mg·g^{-1} for biochar from spent coffee grounds to nearly 800 mg·g^{-1} for advanced MOF materials. Such variability arises from differences in surface area, pore size distribution, functional groups, and adsorbent chemistry.

The AC developed in this work shows an experimental adsorption capacity of 445 mg·g^{-1}, which remains high compared to many bio-based carbons. These results are in line with those reported in the article [42] ,which showed a specific surface area of 47 m²·g^{-1} and a maximum adsorption capacity of 433 mg·g^{-1}.

As a result, in addition to porosity, the surface functional groups introduced play a dominant role in DCF adsorption. Overall, the SCG-AC provides a cost-effective, sustainable, and competitive alternative to conventional adsorbents for pharmaceutical pollutant removal.

Table 5 Comparison of DCF adsorption capacities (q_{max} or q_{exp}) of various adsorbents reported in the literature

Adsorbent type	Adsorption capacity (mg·g^{-1})	Experimental conditions	Ref
AC from SCG	445	[DCF] = 20 mg·L^{-1}; adsorbent dose = 0.2 g·L^{-1}	This work
rGO	59.7	Adsorption at 25 °C; surface-π interactions; mainly physisorption	[43]
MOFs	792	Highly porous metal–organic framework; optimal conditions at pH 6–7	[44]
Thermo-plasma expanded graphite	433	10 mg of TPEG to 50 mL of DCF solution (100 mg L^{-1})	[42]
AC from sugarcane bagasse	315	Chemically activated with H₃PO₄; high surface area; strong π–π interaction	[45]
Biochar from SCG	38.5	Non-activated biochar; moderate surface area; physisorption predominant	[46]

3.3 Removal of DCF using Nanofiltration (NF)

The tests on the treatment of DCF solution ([DCF]= 20 mg. L^{-1})using NF were conducted at various TMP of 4,6 and 8 bar (Figure 11). The results indicate that the permeate flux decreased slightly during the 20 first minutes and then remains almost constant and thatthe permeate flux increases with TMP, showing values from 30.21 L.h^{-1}.m² at 4 bar to 58.14 L.h^{-1}.m² at 8 bar. This behavior indicated that the mass transfer is controlled by the convection for the interval of studied pressures. It is important to notice that the fouling phenomena is not important and can be attributed to the difference of sizes between the DCF and the membrane pores, 318.1 g. mole^{-1} for DCF and almost 200 Da (200 g. mole^{-1}) for NF 270 membrane.

Figure 12 shows that the NF membrane water permeability after rinsing has a value of almost 7 L. h^{-1}.m^{-2}, very near the values obtained during the DCF filtration, supporting that the fouling phenomena is insignificant. The NF membrane achieves a total removal of DCF at 6 and 8 bars and 97% removal at 4 bars. This slight difference can be explained by the increase in the pressure leading to higher DCF rejection.
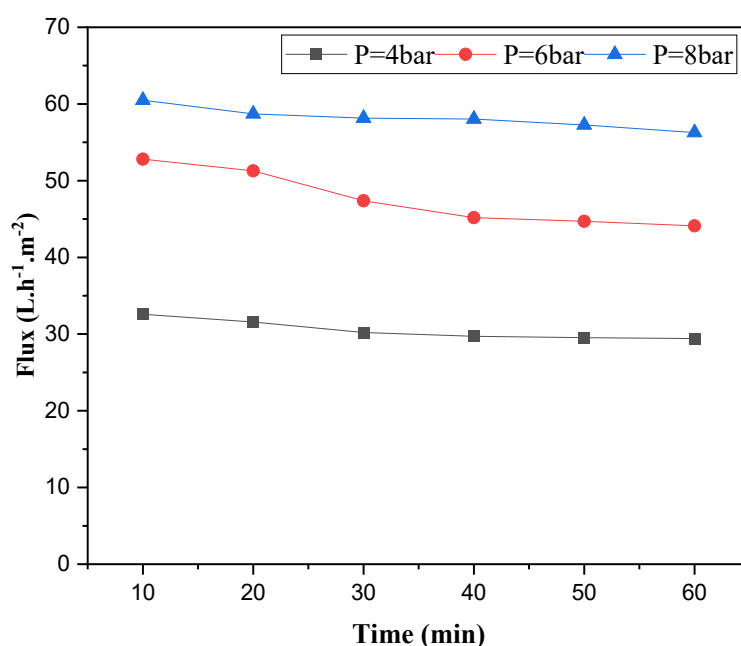

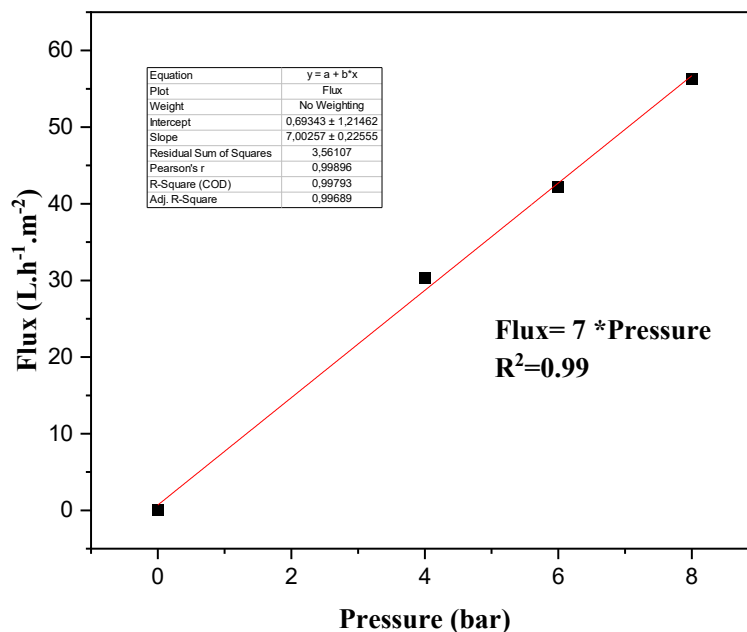**Figure 11** Variation in filtration flux of NF as a function of Time

Equation	y = a + b*x
Plot	Flux
Weight	No Weighting
Intercept	0,69343 ± 1,21462
Slope	7,00257 ± 0,22555
Residual Sum of Squares	3,56107
Pearson's r	0,99896
R-Square (COD)	0,99793
Adj. R-Square	0,99689

Flux= 7 *Pressure
R^2=0.99

Figure 12 Water permeability of the NF membrane

3.4 Comparing the Removal of DCF by Photocatalysis, Adsorption and NF

This analysis compares three advanced water treatment technologies; photocatalysis, adsorption, and NF, based on their effectiveness in removing DCF. Each technology demonstrates unique advantages and operational parameters that contribute to overall wastewater treatment efficiency, but they also show some differ in terms of cost and performance. Photocatalysis applies light-activated catalysts (TiO_2), to degrade organic pollutants. The TiO_2/UV system achieved a total DCF removal within 180 minutes under optimal conditions (1 g. L^{-1} TiO_2 loading and a natural pH of 5). This method is advantageous due to its high efficiency and minimal chemical usage, which reduces the operation cost and the risk of secondary pollution. However, it requires specific light conditions and may face limitations from catalyst deactivation over time. In terms of cost, while specific data for photocatalysis was not

provided in the search results, it is generally considered to have moderate operational costs due to the need for UV light sources and catalyst regeneration [47].

On the other hand, adsorption involves the accumulation of pollutants on solid adsorbents. The SCG adsorbent demonstrated a high adsorption capacity of 100 mg. g^{-1} for DCF, exhibited a 100% removal at an optimal dosage of 0.2 g. L^{-1}. This technology is flexible in operational conditions and has exhibited improved economic viability compared to other technologies [48]. However, it does require periodic replacement or regeneration of adsorbents, which can add to operational costs. Additionally, it can face the risk of generating secondary effluent that may contain residual contaminants if the SCG saturates. This can compromise treatment effectiveness and necessitate additional processes to ensure compliance with environmental standards.

NF is a membrane-based separation process that effectively retains larger

molecules while allowing smaller ones to pass through. NF also achieved complete removal of DCF at pressures of 6 and 8 bars. This method offers continuous operation and high throughput while being effective for various contaminants. In terms of cost, NF processes are often comparable or lower than conventional treatment methods for small facilities. However, they generate a waste stream comprising at least 10% of the feed water volume, which can complicate treatment processes and increase disposal costs [49]. The second effluent quality from NF is typically high, but membrane fouling can lead to increased maintenance costs and reduced efficiency over time.

In conclusion, while all three methods exhibit significant effectiveness in removing DCF from wastewater, photocatalysis stands out for its high efficiency under optimal conditions, its ability to avoid the generation of a second pollution and its capacity to complete remove the pollutants by degradation not just elimination. Adsorption offers a cost-effective solution with flexibility but requires careful management of adsorbent saturation to maintain performance[50]. NF provides robust removal capabilities but may incur higher operational complexities due to waste generation and fouling issues. Ultimately, the choice among these technologies should consider specific wastewater characteristics, economic factors, and operational constraints, with an integrated approach potentially enhancing overall treatment efficacy by leveraging the strengths of each technology for comprehensive pollutant removal in wastewater treatment systems.

4.0 CONCLUSION

This study conducted a comprehensive evaluation of the effectiveness of three advanced water treatment methods: photocatalysis, adsorption, and NF for the removal of DCF, an emerging contaminant frequently detected in wastewater. TiO_2/UV system exhibited a high efficiency removal of DCF of 100% after 180 min at optimal conditions of TiO_2 loading of 1g. L^{-1} and at natural pH (pH=5). In the case of adsorption by SCG, these AC showed a high efficiency in the removal of DCF with (Capacity =100 mg.g^{-1}). The Langmuir model was found to describe the adsorption behavior of DCF on SCG with optimal removal occurring an SCG dosage of 0.2 g. L^{-1}. Increasing the SCG dosage enhanced the adsorption efficiency, achieving up to 100%of DCF removal. On the other hand, NF was effective in the removal of DCF under the different pressures operated with a removal of 100% for 6 and 8 bars (Table 6). While this study focused on evaluating each method individually, the comparative analysis provides valuable insights into their respective performance and potential applicability. The combination of advanced treatment techniques such as adsorption, photocatalysis, and nanofiltration presents a promising approach to enhancing the overall efficiency of wastewater treatment processes. Based on the high removal efficiencies observed, future research should aim to investigate integrated or sequential configurations of these techniques to further improve contaminant removal and treatment reliability.

Table 6 Operating conditions and performances of the three treatment methods for DCF removal

Process	Operating conditions	Measured parameters	Optimal performances
Photocatalysis (TiO₂/UV)	TiO₂ P25 dose = 1 g·L⁻¹; UV-A lamp 18 W; [DCF] = 20 mg·L⁻¹; pH = 3,5,7,9,11	Degradation efficiency (%) after 180 min; kinetic constant (k_{app})	100% removal at pH= 5.3, Dose of TiO₂ =1 g. L⁻¹ and [DCF]= 20 mg. L⁻¹
Adsorption (AC)	AC dose = 0.2 g·L⁻¹; [DCF] = 20 mg·L⁻¹; contact time = 60 min; pH= 1-10	Experimental adsorption capacity ($q_{e,exp}$); removal efficiency (%)	$q_{e,exp}$= 100 mg·g⁻¹; Langmuir q_{max} = 445 mg·g⁻¹; 100% removal
NF	NF270 polyamide membrane; TMP = 4–8 bar; feed volume = 30 L; T ≈ 25 °C	Permeate flux (L·h⁻¹·m⁻²); rejection (%)	Flux = 30.2 L.h⁻¹.m²at 4 bars and 58.1 L.h⁻¹.m²at 8 bar. 100% rejectionat 6 band 8 bar

CONFLICTS OF INTEREST

The authors declare that there is no conflict of interest regarding the publication of this paper.

REFERENCES

[1] Ruziwa, D. T., *et al.* (2023). Pharmaceuticals in wastewater and their photocatalytic degradation using nano-enabled photocatalysts. *Journal of Water Process Engineering, 54*, 103880. https://doi.org/10.1016/j.jwpe.2023.103880.

[2] Vasilachi, I., Asiminicesei, D., Fertu, D., & Gavrilescu, M. (2021). Occurrence and fate of emerging pollutants in water environment and options for their removal. *Water, 13*(2), 181. https://doi.org/10.3390/w13020181.

[3] Aguinaco, A., Beltrán, F. J., García-Araya, J. F., & Oropesa, A. (2012). Photocatalytic ozonation to remove the pharmaceutical diclofenac from water: Influence of variables. *Chemical Engineering Journal, 189–190*, 275–282. https://doi.org/10.1016/j.cej.2012.02.072.

[4] Moctezuma, E., Leyva, E., Lara-Pérez, C., Noriega, S., & Martínez-Richa, A. (2020). TiO₂ photocatalytic degradation of diclofenac: Intermediates and total reaction mechanism. *Topics in Catalysis, 63*(5–6), 601–615. https://doi.org/10.1007/s11244-020-01262-7

[5] Scheurell, M., Franke, S., Shah, R. M., & Hühnerfuss, H. (2009). Occurrence of diclofenac and its metabolites in surface water and effluent samples from Karachi, Pakistan. *Chemosphere, 77*(6), 870–876. https://doi.org/10.1016/j.chemosphere.2009.07.066

[6] Bonnefille, B., Gomez, E., Courant, F., Escande, A., & Fenet, H. (2018). Diclofenac in the marine environment: A review of its occurrence and effects. *Marine Pollution Bulletin, 131*, 496–506. https://doi.org/10.1016/j.marpolbul.2018.04.053.

[7] Nieto-Sandoval, J., Munoz, M., De Pedro, Z. M., & Casas, J. A. (2019). Catalytic hydrodechlorination as polishing step in drinking water treatment for the removal of chlorinated micropollutants. *Separation and Purification Technology, 227*, 115717. https://doi.org/10.1016/j.seppur.2 019.115717.

[8] Sathishkumar, P., Meena, R. A. A., Palanisami, T., Ashokkumar, V., Palvannan, T., & Gu, F. L. (2020). Occurrence, interactive effects and ecological risk of diclofenac in environmental compartments and biota: A review. *Science of the Total Environment, 698*, 134057. https://doi.org/10.1016/j.scitoten v.2019.134057.

[9] Ziylan, A., & Ince, N. H. (2011). The occurrence and fate of anti-inflammatory and analgesic pharmaceuticals in sewage and fresh water: Treatability by conventional and non-conventional processes. *Journal of Hazardous Materials, 187*(1–3), 24–36. https://doi.org/10.1016/j.jhazmat. 2011.01.057.

[10] Hartmann, J., *et al*. (2008). Degradation of the drug diclofenac in water by sonolysis in presence of catalysts. *Chemosphere, 70*(3), 453–461. https://doi.org/10.1016/j.chemos phere.2007.06.063

[11] Zhang, Y., Geißen, S.-U., & Gal, C. (2008). Carbamazepine and diclofenac: Removal in wastewater treatment plants and occurrence in water bodies. *Chemosphere, 73*(8), 1151–1161. https://doi.org/10.1016/j.chemos phere.2008.07.086

[12] Zhou, Y., *et al.* (2017). Insight into highly efficient co-removal of p-nitrophenol and lead by nitrogen-functionalized magnetic ordered mesoporous carbon: Performance and modelling. *Journal of Hazardous Materials, 333*, 80–87. https://doi.org/10.1016/j.jhazmat. 2017.03.031.

[13] Mohan, H., *et al*. (2022). Highly efficient visible light photocatalysis of NiZnFe$_2$O$_4$ nanoparticles: Diclofenac degradation mechanism and eco-toxicity. *Chemosphere, 301*, 134699. https://doi.org/10.1016/j.chemos phere.2022.134699.

[14] Tiwari, B., Drogui, P., & Tyagi, R. D. (2020). Removal of emerging micro-pollutants from pharmaceutical industry wastewater. In *Current Developments in Biotechnology and Bioengineering* (pp. 457–480). Elsevier. https://doi.org/10.1016/B978-0-12-819594-9.00018-8.

[15] Revilla, C., *et al.* (2025). Enhancing antibiotic degradation via photocatalysis and hydrodynamic cavitation using TiO$_2$ catalyst supported on aluminum sludge. *Environmental Technology & Innovation, 37*, 104030. https://doi.org/10.1016/j.eti.2025 .104030

[16] Issaoui, M., & Limousy, L. (2018). Low-cost ceramic membranes: Synthesis, classifications, and applications. *Comptes Rendus Chimie, 22*(2–3), 175–187. https://doi.org/10.1016/j.crci.201 8.09.014.

[17] Cui, Z., Peng, W., Fan, Y., Xing, W., & Xu, N. (2013). Ceramic membrane filtration as seawater RO pre-treatment: Influencing factors on the ceramic membrane

flux and quality. *Desalination and Water Treatment, 51*(13–15), 2575–2583. https://doi.org/10.1080/19443994 .2012.749025.

[18] Benitez, F. J., Real, F. J., Acero, J. L., & Garcia, C. (2007). Kinetics of the transformation of phenyl-urea herbicides during ozonation of natural waters. *Water Research, 41*(18), 4073–4084. https://doi.org/10.1016/j.watres.2 007.05.041.

[19] Dun, R., *et al.* (2024). Nanofiltration membrane fouling control and cleaning efficiency of micro- and nanobubbles. *Desalination and Water Treatment, 317,* 100297. https://doi.org/10.1016/j.dwt.202 4.100297.

[20] Mohd Hanafiah, Z., *et al.* (2024). Removal of pharmaceutical compounds from sewage effluent by the nanofiltration membrane. *Journal of Water Process Engineering, 68,* 106320. https://doi.org/10.1016/j.jwpe.20 24.106320.

[21] Cristóvão, M. B., *et al.* (2019). Treatment of anticancer drugs in hospital and wastewater effluents using nanofiltration. *Separation and Purification Technology, 224,* 273–280. https://doi.org/10.1016/j.seppur.2 019.05.016.

[22] Nayak, V., Cuhorka, J., & Mikulášek, P. (2022). Separation of drugs by commercial nanofiltration membranes and their modelling. *Membranes, 12*(5), 528. https://doi.org/10.3390/membran es12050528.

[23] Almeida-Naranjo, C. E., Guerrero, V. H., & Villamar-Ayala, C. A. (2023). Emerging contaminants and their removal from aqueous media using various adsorbents. *Water, 15*(8), 1626. https://doi.org/10.3390/w150816 26

[24] Saratale, G. D., *et al.* (2020). Valorization of spent coffee grounds towards biopolymers and biocatalysts production. *Bioresource Technology, 314,* 123800. https://doi.org/10.1016/j.biortech .2020.123800.

[25] Aouay, F., Afef, A., Damak, L., Ben Amar, R., & Deratani, A. (2024). Activated carbon prepared from waste coffee grounds: Characterization and adsorption properties of dyes. *Preprints.* https://doi.org/10.20944/preprint s202405.0964.v1.

[26] Saratale, G. D., *et al.* (2020). Valorization of spent coffee grounds towards biopolymers and biocatalysts production. *Bioresource Technology, 314,* 123800. https://doi.org/10.1016/j.biortech .2020.123800.

[27] Salah, Z., Aloulou, H., Bhattacharyya, S., Algieri, C., & Ben Amar, R. (2025). Potential elimination of diclofenac sodium using orange peel waste-based activated carbon. *Euro-Mediterranean Journal for Environmental Integration, 10*(4), 2127–2143. https://doi.org/10.1007/s41207-025-00822-1.

[28] Wu, L., Du, C., He, J., Yang, Z., & Li, H. (2020). Effective adsorption of diclofenac sodium by lignite activated cokes. *Journal of Hazardous Materials, 384,* 121284. https://doi.org/10.1016/j.jhazmat. 2019.121284.

[29] Joseph, A., Yelekar, G. R., & Vijayanandan, A. (2024). Carbamazepine removal using TiO₂–reduced graphene oxide: Adsorption, photocatalysis, and ultrafiltration. *Applied Catalysis A: Open, 193*, 206967. https://doi.org/10.1016/j.apcato.2024.206967.

[30] Ben Salah, S., *et al.* (2024). Treatment of real textile effluent containing indigo dye using hybrid adsorption–membrane system. *Frontiers in Membrane Science and Technology, 3*, 1348992. https://doi.org/10.3389/frmst.2024.1348992.

[31] Rizzo, L., *et al.* (2009). Degradation of diclofenac by TiO₂ photocatalysis: UV absorbance kinetics and toxicity evaluation. *Water Research, 43*(4), 979–988. https://doi.org/10.1016/j.watres.2008.11.040.

[32] Reza, K. M., Kurny, A., & Gulshan, F. (2017). Parameters affecting photocatalytic degradation of dyes using TiO₂: A review. *Applied Water Science, 7*(4), 1569–1578. https://doi.org/10.1007/s13201-015-0367-y.

[33] Gao, L., *et al.* (2020). Effect of dissolved organic matter and ions on TiO₂ photocatalysis of diclofenac. *Environmental Science and Pollution Research, 27*(2), 2044–2053. https://doi.org/10.1007/s11356-019-06676-9.

[34] Bediako, J. K., Affrifah, N. S., Yun, Y.-S., & Repo, E. (2025). Optimization of aurocyanide adsorption on biomass activated carbon. *Minerals Engineering, 227*, 109293. https://doi.org/10.1016/j.mineng.2025.109293.

[35] Sellaoui, L., *et al.* (2023). Adsorption of emerging pollutants on lignin-based activated carbon: Mechanism analysis. *Chemical Engineering Journal, 452*, 139399. https://doi.org/10.1016/j.cej.2022.139399.

[36] Kocabıyık, B., Üner, O., & Geçgel, Ü. (2024). Diclofenac adsorption using activated carbon from einkorn husk. *Adsorption, 30*(6), 1033–1046. https://doi.org/10.1007/s10450-024-00479-2.

[37] Peñafiel, M. E., *et al.* (2024). Enhancing diclofenac removal using acid-treated zeolite. *Case Studies in Chemical and Environmental Engineering, 9*, 100575. https://doi.org/10.1016/j.cscee.2023.100575.

[38] Salman, S. D., Rasheed, I. M., & Ismaeel, M. M. (2023). Diclofenac removal using apricot seed activated carbon. *Chemical Data Collections, 43*, 100982. https://doi.org/10.1016/j.cdc.2022.100982.

[39] dos Reis, G. S., *et al.* (2024). Sustainable sulfur-doped carbon for diclofenac removal. *Environmental Research, 251*, 118595. https://doi.org/10.1016/j.envres.2024.118595.

[40] Kumar, A., Patra, C., Rajendran, H. K., & Narayanasamy, S. (2022). Activated carbon–chitosan adsorbent for diclofenac removal. *Chemosphere, 307*, 135806. https://doi.org/10.1016/j.chemosphere.2022.135806

[41] Yu, H., *et al.* (2025). Adsorption mechanism of arsenic(V) on aged polyethylene microplastics. *Journal of Hazardous Materials Advances, 18*, 100711.

https://doi.org/10.1016/j.hazadv.2025.100711.

[42] Cuccarese, M., *et al*. (2021). Removal of diclofenac by thermo-plasma expanded graphite. *Scientific Reports, 11*(1), 3427. https://doi.org/10.1038/s41598-021-83117-z.

[43] Jauris, I. M., *et al*. (2016). Adsorption of sodium diclofenac on graphene. *Physical Chemistry Chemical Physics, 18*(3), 1526–1536. https://doi.org/10.1039/C5CP05940B.

[44] Prasetya, N., & Wöll, C. (2023). Removal of diclofenac using Zr-MOFs. *RSC Advances, 13*(33), 22998–23009. https://doi.org/10.1039/D3RA03527A.

[45] Sandoval-González, A., Robles, I., Pineda-Arellano, C. A., & Martínez-Sánchez, C. (2022). Removal of anti-inflammatory drugs using agro-industrial activated carbon. *Journal of the Iranian Chemical Society, 19*(10), 4017–4033. https://doi.org/10.1007/s13738-022-02588-7.

[46] Zungu, V., Gumbi, B., & Chen, C. (2022). Fabrication of biochar from coffee grounds and its efficiency for removing pharmaceuticals. *ResearchGate*. https://doi.org/10.13140/RG.2.2.29534.92480.

[47] Gar Alalm, M., Tawfik, A., & Ookawara, S. (2015). Solar TiO_2 photocatalysis vs. solar photo-Fenton for pesticide wastewater. *Journal of Water Process Engineering, 8*, 55–63. https://doi.org/10.1016/j.jwpe.2015.09.007

[48] Pryce, D., *et al*. (2022). Life-cycle cost analysis of technologies for removing emerging contaminants. *Water, 14*(12), 1919. https://doi.org/10.3390/w14121919.

[49] Franke, V., *et al*. (2021). Combining nanofiltration, GAC, and AER for PFAS removal. *ACS ES&T Water, 1*(4), 782–795. https://doi.org/10.1021/acsestwater.0c00141.

[50] Mechnou, I., *et al*. (2025). Activated carbons for pharmaceutical adsorption: Factors and cost analysis. *Results in Engineering, 27*, 105966. https://doi.org/10.1016/j.rineng.2025.105966.